

# Spatial Entropy Regularization for Vision Transformers

**Elia Peruzzo**

University of Trento

[elia.peruzzo@unitn.it](mailto:elia.peruzzo@unitn.it)

**Enver Sangineto\***

University of Modena and Reggio Emilia

[enver.sangineto@unimore.it](mailto:enver.sangineto@unimore.it)

**Yahui Liu\***

University of Trento

Fondazione Bruno Kessler

[yahui.liu@unitn.it](mailto:yahui.liu@unitn.it)

**Marco De Nadai**

Fondazione Bruno Kessler

[work@marcodena.it](mailto:work@marcodena.it)

**Wei Bi**

Tencent AI Lab

[victoriabi@tencent.com](mailto:victoriabi@tencent.com)

**Bruno Lepri**

Fondazione Bruno Kessler

[lepri@fbk.eu](mailto:lepri@fbk.eu)

**Nicu Sebe**

University of Trento

[niculae.sebe@unitn.it](mailto:niculae.sebe@unitn.it)

## Abstract

Recent work has shown that the attention maps of Vision Transformers (VTs), when trained with self-supervision, can contain a semantic segmentation structure which does not spontaneously emerge when training is supervised. In this paper, we *explicitly* encourage the emergence of this spatial clustering as a form of training regularization, this way including a self-supervised *pretext task* into the standard supervised learning. In more detail, we propose a VT regularization method based on a spatial formulation of the information entropy. By minimizing the proposed spatial entropy, we explicitly ask the VT to produce “spatially ordered” attention maps, this way including an *object-based prior* during training. Using extensive experiments, we show that the proposed regularization approach is beneficial with different training scenarios, datasets, downstream tasks and VT architectures. The code will be available upon acceptance.

## 1 Introduction

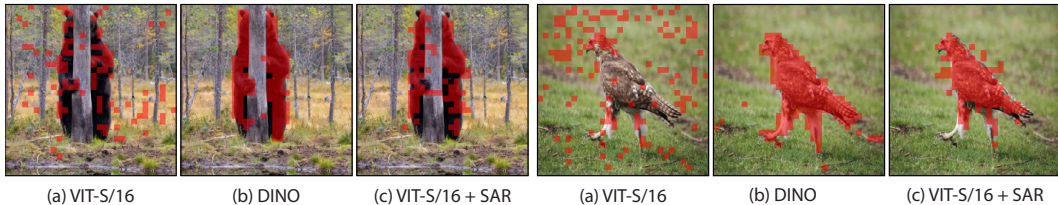


Figure 1: ViT attention maps obtained using the [CLS] token query and thresholded to keep 60% of the mass (as proposed in [14]). (a) Supervised learning: the higher attention values (red) are spread over the whole image. (b) The attention map of DINO [14], in which a semantic segmentation structure *spontaneously* emerges after self-supervised training. (c) Training using the proposed SAR, which *explicitly* encourages the emergence of spatially clustered regions.

\*Equally contributors.

There is a growing interest in the computer vision community on Vision Transformers (VTs), as a computational paradigm alternative to standard Convolutional Neural Networks (CNNs). VTs are inspired by the Transformer network [69], which is the *de facto* standard in Natural Language Processing (NLP) [22, 57], and it is based on multi-head attention layers transforming the input *tokens* (e.g., language words) into a set of final embedding tokens. Dosovitskiy *et al.* [24] recently proposed an analogous processing paradigm, where word tokens are replaced by image patches, and self-attention layers are used to model global pairwise dependencies over all the input tokens. As a consequence, differently from CNNs, where the convolutional kernels have a spatially limited receptive field, ViT [24] has a dynamic receptive field, which is given by its attention maps [53]. However, ViT heavily relies on huge training datasets (e.g., JFT-300M [24], a proprietary dataset of 303 million images), and underperforms CNNs when trained on ImageNet-1K ( $\sim 1.3$  million images [63]) or using smaller datasets [24, 58]. To mitigate the need for a huge quantity of training data, a recent line of research is exploring the possibility of reintroducing typical CNN mechanisms in VTs [77, 49, 73, 76, 75, 47, 41]. The main idea behind these works is that convolutional layers, mixed with the VT self-attention layers, help to embed a *local inductive bias* in the VT design, i.e., to encourage the network to focus on local properties of the image domain. In this paper, we follow an orthogonal (and relatively simpler) direction, and we propose a training *regularization* method which can be easily plugged into existing VTs without making significant structural changes to their architectures. Specifically, we encourage the VT to produce attention maps which focus on local regions (of *variable size*), based on the idea that, most of the time, an object is represented by a spatially connected region in the input image.

Our work is inspired by the findings presented in [14, 6, 53], in which the authors show that VTs, trained using self-supervision [14, 6] or shape-distillation [53], can spontaneously develop attention maps with a semantic segmentation structure. For instance, Caron *et al.* [14] show that the last-layer attention maps of ViT, when this is trained with their self-supervised DINO algorithm, can be thresholded and used to segment the most important foreground objects of the input image *without any pixel-level annotation* during training (see Fig. 1 (b)). Similar findings are shown in [6, 53]. Interestingly, however, Caron *et al.* [14] show that the same ViT architectures, when trained with supervised methods, produce much more spatially disordered attention maps (Fig. 1 (a)). This is confirmed by Neimark *et al.* [53], who observed that the attention maps of ViT, trained with supervised protocols, have a widely spread structure over the whole image. The reason why “blob”-like attention maps *spontaneously* emerge, when VTs are trained with some algorithms but not with others, is still unclear. However, in this paper we build on top of these findings and we propose a *spatial entropy* loss function which *explicitly* encourages the emergence of locally structured attention maps (Fig. 1 (c)), independently of the main algorithm used for training. The resulting method is a mix of standard supervised and *self-supervised* training, in which the minimization of the proposed spatial entropy loss acts as a *pretext task* to extract information from images without additional supervision. In this way, we can include an *object-based local prior* during training and alleviate the need for huge supervised training datasets, without changing the main VT architecture design.

The second contribution of this paper is based on the empirical results very recently presented by Raghu *et al.* [58], who showed that VTs are more influenced by the skip connections than CNNs and, specifically, that in the last blocks of ViT, the *patch tokens* (see §3) representations are mostly influenced by the skip connection path. This means that, in the last blocks of ViT, the self-attention layers have a relatively small influence on the final token embeddings. Since our goal is to emphasize the role of the spatial information represented by the attention maps, we propose to remove the skip connections in the last block (only). We empirically show that this minor architectural change is beneficial for ViT, both when used jointly with our spatial entropy loss, and when used with a standard training procedure.

Our regularization method, which we call SAR (Spatial Attention-based Regularization), can be easily plugged into existing VTs without drastic architectural changes and it can be applied to different scenarios, jointly with a main-task loss function. For instance, when used in a supervised classification task, the main loss is the (standard) cross entropy, used jointly with our spatial entropy loss. Note that the latter extracts information from the attention maps in an unsupervised way, without requiring additional annotation information. In summary, our main contributions are the followings: (1) We propose a spatial entropy loss for VT training regularization, which explicitly encourages the generation of attention maps spatially clustered; (2) We propose to remove the last-block skip connections, empirically showing that this is beneficial for the patch token representations; (3) Using

extensive experiments, we show that SAR improves the accuracy of different VT architectures, both when trained from scratch and when fine-tuned.

## 2 Related work

**Vision Transformers.** One of the very first fully-Transformer architectures for computer vision is iGPT [15], in which each image pixel is represented as a token. However, due to the quadratic computational complexity of Transformer networks [69], iGPT can only operate with very small resolution images. This problem has been largely alleviated by ViT [24], where the input tokens are  $p \times p$  image patches (§3). The success of ViT has inspired several similar Vision Transformer (VT) architectures in different application domains, such as image classification [24, 66, 77, 49, 73, 76, 47, 75, 21], object detection [11, 82, 20], segmentation [64, 60], human pose estimation [80], object tracking [52], video processing [54, 46], image generation [43, 41], point cloud processing [32, 79], and many others. However, the lack of the typical CNN local inductive biases makes VTs to need more data for training [24, 58]. For this reason, many recent works are addressing this problem by proposing hybrid architectures, which reintroduce typical convolutional mechanisms into the VT design [77, 49, 73, 76, 75, 47, 21, 41, 46]. In contrast, we propose a different and simpler solution, in which we regularize the VT training by explicitly encouraging the emergence of spatially connected regions of high attention values. This way, we introduce a local prior (“objects usually correspond to connected image components”) without substantially changing the structure of the VT, apart from the last-block skip connection removal.

**Self-supervised learning.** Most of the self-supervised approaches with still images impose a semantic consistency between different views of the same image, where the views are obtained with data-augmentation techniques. So far, most of the research in this field has been based on ResNet [35] backbones, and can be roughly grouped in contrastive learning [68, 38, 16, 34, 65, 70, 25], clustering methods [9, 83, 42, 12, 2, 29, 13, 14], asymmetric networks [31, 18] and feature-decorrelation methods [27, 78, 7, 40]. In the last year, many articles have appeared which use VTs for self-supervised learning. For instance, Chen *et al.* [19] have empirically tested different representatives of the above categories using VTs, and they also proposed MoCo-v3, a contrastive approach based on MoCo [34] but without the queue of the past-samples. DINO [14] is an on-line clustering method which is one of the current state-of-the-art self-supervised approaches using VTs. BEiT [6] adopts the typical “masked-word” NLP pretext task [22, 57], but it needs to pre-extract a vocabulary of image words using the discrete VAE pre-trained in [59]. Other very recent works which use a “masked-patch” pretext task are [33, 74, 72, 23, 39, 17, 3, 26, 81, 44].

In this paper, we do not propose a new self-supervised algorithm, but we rather use self-supervision (we extract information from samples without additional manual annotation) to speed-up the convergence in a supervised scenario. In the Supplementary Material, we also show that SAR can be plugged on top of both MoCo-v3 and DINO, boosting the accuracy of both of them. Finally, similarly to this paper, Liu *et al.* [48] propose a VT regularization approach based on predicting the geometric distance between patch tokens, but they focus on VT training using small-medium datasets and they use only hybrid VT architectures.

**Spatial entropy.** There are many definitions of spatial entropy [61, 1]. For instance, Batty [8] normalizes the probability of an event occurring in a given zone by the area of that zone, this way accounting for unequal space partitions. In [67], spatial entropy is defined over a Markov Random Field describing the image content, but its computation is very expensive [61]. In contrast, our spatial entropy loss can be efficiently computed and it is differentiable, thus it can be easily used as an auxiliary regularization task in existing VTs.

## 3 Background

Given an input image  $I$ , Dosovitskiy *et al.* [24] split  $I$  in a grid of  $K \times K$  non-overlapping patches, and each patch is linearly projected into a (learned) input embedding space. The input of ViT is this set of  $n = K^2$  *patch tokens*, jointly with a special token, called [CLS] token, which is used to represent the whole image. Following a standard Transformer network [69], ViT [24] transforms these  $n + 1$  tokens in corresponding final  $n + 1$  token embeddings using a sequence of  $L$  Transformer blocks. Each block is composed of LayerNorm (LN), Multiheaded Self Attention (MSA) and MLP

layers, plus skip connections. Specifically, if the token embedding sequence at the  $(l - 1)$ -th layer is  $\mathbf{z}^{l-1} = [\mathbf{z}_{CLS}; \mathbf{z}_1; \dots; \mathbf{z}_n]$ , then:

$$\mathbf{z}' = \text{MSA}(\text{LN}(\mathbf{z}^{l-1})) + \mathbf{z}^{l-1}, \quad l = 1, \dots, L \quad (1)$$

$$\mathbf{z}^l = \text{MLP}(\text{LN}(\mathbf{z}')) + \mathbf{z}', \quad l = 1, \dots, L \quad (2)$$

where the addition (+) denotes a skip (or “identity”) connection, which is used both in the MSA (Eq. 1) and in the MLP (Eq. 2) layer. The MSA layer is composed of  $H$  different heads, and in the  $h$ -th head ( $1 \leq h \leq H$ ), each token embedding  $\mathbf{z}_i \in \mathbb{R}^d$  is projected into a query ( $\mathbf{q}_i^h$ ), a key ( $\mathbf{k}_i^h$ ) and a value ( $\mathbf{v}_i^h$ ). Given query ( $Q^h$ ), key ( $K^h$ ) and value ( $V^h$ ) matrices containing the corresponding elements, the  $h$ -th self-attention matrix ( $A^h$ ) is:

$$A^h = \text{softmax} \left( \frac{Q^h (K^h)^T}{\sqrt{d}} \right). \quad (3)$$

Each head outputs a weighted sum of the values in  $V^h$ , using  $A^h$  for the weights. The final MSA layer output is obtained by concatenating all the head outputs and then projecting each token embedding into a  $d$ -dimensional space. Finally, the last-layer ( $L$ ) class token embedding  $\mathbf{z}_{CLS}^L$  is fed to an MLP head, which computes a posterior distribution over the set of the target classes and the whole network is trained using a standard cross-entropy loss ( $\mathcal{L}_{ce}$ ). Some hybrid VTs (see §2) such as CvT [73] and PVT [71], progressively subsample the number of patch tokens, leading to a final  $k \times k$  patch token grid ( $k \leq K$ ). In the rest of this paper, we generally refer to a spatially arranged grid of final patch token embeddings with a  $k \times k$  resolution.

## 4 Method

Generally speaking, an object usually corresponds to one or very few connected regions of a given image (Fig. 1). Our goal is to exploit this natural image prior and penalize those attention maps which do not lead to a spatial clustering of their larger values. Intuitively, if we compare Fig. 1 (a) with Fig. 1 (b), we observe that, in the latter case, the attention maps are more “spatially ordered”, i.e. there are *less* and *bigger* “blobs” (obtained after thresholding the map values [14]). Since an image is usually composed of a few main objects, each of which most of the times is represented as a connected region of tokens, during training we penalize those attention maps which produce a large number of small blobs. We use this as an auxiliary pretext task which extracts information from images without additional annotation, by exploiting the assumption that spatially close tokens should preferably belong to the same cluster.

### 4.1 Spatial entropy loss

For each head  $h$  of the last Transformer block ( $L$ , see §3), we compute a similarity map  $S^h$  by comparing the [CLS] token query ( $\mathbf{q}_{CLS}^h$ ) with all the patch token keys ( $\mathbf{k}_{x,y}^h$ , where  $(x, y) \in \{1, \dots, k\}^2$ ):

$$S_{x,y}^h = \langle \mathbf{q}_{CLS}^h, \mathbf{k}_{x,y}^h \rangle / \sqrt{d}, \quad (x, y) \in \{1, \dots, k\}^2, \quad (4)$$

where  $\langle \mathbf{a}, \mathbf{b} \rangle$  is the dot product between  $\mathbf{a}$  and  $\mathbf{b}$ .  $S^h$  is extracted from the self-attention map  $A^h$  by selecting the [CLS] token as the only query and before applying the softmax (see §4.3 for a discussion about this choice).  $S^h$  is a  $k \times k$  matrix corresponding to the final  $k \times k$  spatial grid of patches (§3), and  $(x, y)$  corresponds to the “coordinates” of a patch token in this grid.

In order to extract a set of connected components containing the largest values in  $S^h$ , we zero-out those elements of  $S^h$  which are smaller than the mean value  $m = 1/n \sum_{(x,y) \in \{1, \dots, k\}^2} S_{x,y}^h$ :

$$B_{x,y}^h = \text{ReLU}(S_{x,y}^h - m), \quad (x, y) \in \{1, \dots, k\}^2, \quad (5)$$

where thresholding using  $m$  corresponds to retain half of the total “mass” of Eq. 4. We can now use a standard algorithm [30] to extract the connected components from  $B^h$ , where each component is obtained using an 8-connectivity relation between non-zero elements in  $B^h$  (see Fig. 2):

$$C^h = \{C_1, \dots, C_{h_r}\} = \text{ConnComponents}(B^h). \quad (6)$$

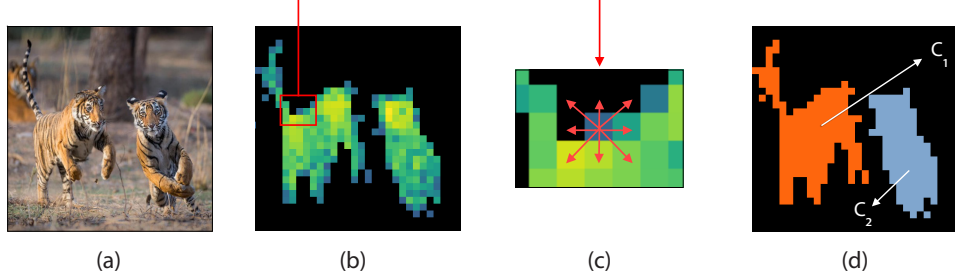


Figure 2: A schematic illustration of the spatial entropy. (a) The original image. (b) The thresholded similarity map  $B^h$  (zero values shown in black). (c) The 8-connectivity relation used to group non-zero elements in  $B^h$ . (d) The resulting two connected components ( $C_1$  and  $C_2$ ), each component shown with a different colour.

$C_j$  ( $1 \leq j \leq h_r$ ) in  $C^h$  is the set of coordinates ( $C_j = \{(x_1, y_1), \dots, (x_{n_j}, y_{n_j})\}$ ) of the  $j$ -th connected component, whose cardinality ( $n_j$ ) is variable, and such is the total number of components ( $h_r$ ). Given  $C^h$ , we define the spatial entropy as:

$$\mathcal{H}(S^h) = - \sum_{j=1}^{h_r} P^h(C_j) \log P^h(C_j), \quad (7)$$

$$P^h(C_j) = \frac{1}{|B^h|} \sum_{(x,y) \in C_j} B_{x,y}^h, \quad (8)$$

where  $|B^h| = \sum_{(x,y) \in \{1, \dots, k\}^2} B_{x,y}^h$ . Importantly, in Eq. 8, the probability of each region ( $P^h(C_j)$ ) is computed using all its elements, and this makes the difference with respect to a non-spatial entropy which is directly computed over all the elements in  $S^h$ , without considering the adjacency relation. Note that the less the number of components  $h_r$  or the less uniformly distributed the probability values  $P^h(C_1), \dots, P^h(C_{h_r})$ , the lower  $\mathcal{H}(S^h)$ . Using Eq. 7, the spatial entropy loss is defined as:

$$\mathcal{L}_{se} = \frac{1}{H} \sum_{h=1}^H \mathcal{H}(S^h). \quad (9)$$

$\mathcal{L}_{se}$  is used jointly with the main task loss. For instance, in case of supervised training, we use:  $\mathcal{L}_{tot} = \mathcal{L}_{ce} + \lambda \mathcal{L}_{se}$ , where  $\lambda$  is the weight given to  $\mathcal{L}_{se}$ .

## 4.2 Removing the skip connections

Very recently, [58] empirically showed that, *in the last blocks* of ViT, the patch token representations are mostly propagated from the previous layers using the skip connections [58] (see §1). We presume this is (partially) due to the fact that only the [CLS] token is used as input to the classification MLP head (see §3), thus the last-block patch token embeddings are usually neglected. Moreover, [58] show that the effective receptive field [51] of each block, when computed *after* the MSA skip connections, is much smaller than the effective receptive field computed *before* the MSA skip connections. Both empirical observations lead to the conclusion that the MSA skip connections in the last blocks may be detrimental for the *representation* capacity of the final patch token embeddings. This problem is emphasized when using our spatial entropy loss, since it is computed using the attention maps of the last-block MSA (§4.1). For these reasons, we propose to remove the MSA skip connections in the last block ( $L$ ). Specifically, in the  $L$ -th block, we replace Eq. 1-2 with:

$$\mathbf{z}' = \text{MSA}(\text{LN}(\mathbf{z}^{L-1})), \quad (10)$$

$$\mathbf{z}^L = \text{MLP}(\mathbf{z}') + \mathbf{z}'. \quad (11)$$

Note that, in addition to removing the MSA skip connections (Eq. 10), we also remove the subsequent LN (Eq. 11), because we empirically observed that this further improves the VT accuracy (see §5.1).

### 4.3 Discussion

In this section, we discuss and motivate some of the choices made in §4.1 and §4.2.

First, we use the similarity map  $S^h$  extracted before the softmax (Eq. 3) because we observed that, using the softmax, the network can “cheat”, by increasing the norm of the vectors  $q_{CLS}$  and  $k_{x,y}$  ( $(x, y) \in \{1, \dots, k\}^2$ ). As a result, the dot product  $\langle q_{CLS}, k_{x,y} \rangle$  also largely increases, and the softmax operation (based on the exponential function) enormously exaggerates the difference between the elements in  $S^h$ , generating a very peaked distribution, which zeros-out non-maxima  $(x, y)$  elements. Basically, when using the softmax, the VT is able to minimize Eq. 9 by producing single-peak similarity maps which have a 0 entropy, each being composed of only one connected component with only one single token (i.e.,  $h_r = 1$  and  $n_j = 1$ ).

Second, the spatial entropy (Eq. 7) is computed for each head separately and then averaged (Eq. 9) to allow each head to focus on *different* image regions. Note that, although computing the connected components (Eq. 6) is a non-differentiable operation,  $C^h$  is only used to “pool” the values of  $B^h$  (Eq. 8), and each  $C_j$  can be implemented as a binary mask (more details in the Supplementary Material, where we also compare  $\mathcal{L}_{se}$  with other solutions).

Finally, we remove the MSA skip connections only in the last block (Eq. 10-11) because, according to the results reported in [58], removing the skip connections in the ViT intermediate blocks, brings to an accuracy drop. In contrast, in §5.1 we show that our strategy, which keeps the ViT architecture unchanged apart from the last block, is beneficial even when used *without* our spatial entropy loss.

In the rest of this paper, we refer to our full method SAR as composed of the spatial entropy loss (§4.1) and the last-block MSA skip connection and LN removal (§4.2).

## 5 Experiments

In §5.1 we analyse the contribution of the spatial entropy loss and the skip connection removal. In §5.2 we show that, using SAR and different VT architectures, we can improve VT training in different scenarios: (1) training from scratch on ImageNet-1K and small/medium datasets, (2) transfer learning on small datasets, (3) robustness with respect to out-of-distribution testing. Finally, in §5.3 we analyse the properties of the attention maps generated using SAR. We train each model using 8 NVIDIA V100 32GB GPUs.

### 5.1 Ablation study

In this section, we analyse the influence of the  $\lambda$  value (§4.1), the removal of the skip connections and the LN in the last VT block (§4.2), and the use of the spatial entropy loss (§4.1). In all the ablation experiments, we use ImageNet-100 (IN-100), [65, 70], which is a subset of 100 classes of ImageNet and ViT-S/16, a 22 million parameter ViT [24], trained with  $224 \times 224$  resolution images and  $14 \times 14$  patches tokens ( $k = 14$ ) with a patch resolution of  $16 \times 16$  [66]. Moreover, in all the experiments in this section, we adopt the training protocol and the data-augmentations described in [49].

In Tab. 1 (a), we train from scratch all the models using 100 epochs and we show the impact on the test set accuracy using different values of  $\lambda$ . In the experiments of this table, we use our loss function ( $\mathcal{L}_{tot} = \mathcal{L}_{ce} + \lambda \mathcal{L}_{se}$ ) and we remove both the skip connections and the LN in the last block (Eq. 10-11), thus the column  $\lambda = 0$  corresponds to the result reported in Tab. 1 (b), Row “C” (see below). In the rest of the paper, we use the results obtained with this setting (IN-100, 100 epochs, etc.) and the best  $\lambda$  value ( $\lambda = 0.01$ ) for **all** the other datasets, training scenarios (e.g., training from scratch or fine-tuning) and VT architectures (e.g., ViT, CvT, PVT, etc.). In fact, although a higher accuracy can very likely be obtained by tuning  $\lambda$ , our goal is to show that SAR is an easy-to-use regularization approach, even without tuning its only hyperparameter.

In Tab. 1 (b), we train from scratch all the models using 100 epochs and Row “A” corresponds to our run of the original ViT-S/16 (Eq. 1-2). When we remove the MSA skip connections (Row “B”), we observe a +0.42 points improvement, which becomes +1.5 if we also remove the LN (Row “C”). This experiment confirms that the last block patch tokens can learn more useful representations if we inhibit the MSA identity path (Eq. 10-11). However, if we also remove the skip connections in the subsequent MLP layer (Row “D”), the results are inferior to the baseline. Finally, when we use the spatial entropy loss with the original architecture (Row “E”), the improvement is marginal, but using

Table 1: ImageNet 100. (a) Influence of the spatial entropy loss weight  $\lambda$  (100 epochs). (b) Analysis of the different components of SAR (100 epochs). (c) Influence of the number of epochs.

<b><math>\lambda</math></b>	<b>Top-1 Acc.</b>	<b>Model</b>	<b>Top-1 Acc.</b>		<b>Top-1 Acc.</b>	
				<b>Model</b>	100 ep.	300 ep.
0	75.72	A: Baseline	74.22			
0.001	75.82	B: A + no MSA skip connections	74.64 (+0.42)			
0.005	76.16	C: B + no LN	75.72 (+1.5)			
0.01	<b>76.72</b>	D: C + no MLP skip connections	73.76 (-0.46)			
0.05	76.22	E: A + spatial entropy loss	74.78 (+0.56)			
0.1	75.88	F: A + SAR	76.72 (+2.5)			

(a)

(b)

(c)

$\mathcal{L}_{se}$  jointly with Eq. 10-11 (full model, Row “F”), the accuracy boost with respect to the baseline is much stronger. Tab. 1 (c) compares training with 100 and 300 epochs and shows that, in the latter case, SAR can reach a much higher relative improvement with respect to the baseline (+4.42). In the Supplementary Material, we use IN-100 to show additional experiments with other VT architectures and we plug SAR on top of self-supervised algorithms (§2).

## 5.2 Main results

**Training from scratch on ImageNet.** We start with a set of experiments on ImageNet-1K (IN-1K), in which we plug SAR into different VT architectures: ViT [24], T2T [77], PVT [71] and CvT [73]. We omit other common frameworks such as, for instance, Swin [49] because of the lack of a [CLS] token in their architecture. Although the [CLS] token used, e.g, in §4.1 to compute  $S^h$ , can potentially be replaced by a vector obtained by average-pooling all the patch embeddings, we leave this for future investigations.

Moreover, for computational reasons, we focus on small-medium capacity VTs (see Tab. 2 for details on the number of parameters of each VT). Importantly, for each tested method, we use the original training protocol developed by the corresponding authors, including the learning rate schedule, the batch size, the VT-specific hyperparameter values and the data-augmentation type used to obtain the corresponding published results (see column “Training Protocol” in Tab. 2). Finally, as mentioned in §5.1, we keep fixed the only SAR hyperparameter ( $\lambda = 0.01$ ). Although better results can likely be obtained by hyperparameter tuning (including the VT-specific hyperparameters), our goal is to show that SAR can be easily used in different VTs increasing their final testing accuracy. The results reported in Tab. 2 show that SAR improves *all* the tested VTs, independently of their specific architecture, model capacity or training protocol. Notably, SAR leads to almost 1 point difference with respect to ViT-S/16 [66], which is obtained *without any additional learnable parameters*. Note that both PVT and CvT have a final embedding grid resolution of  $7 \times 7$ , which is smaller than the  $14 \times 14$  grid used in ViT and T2T, and this probably has a negative impact on our spatial based entropy loss. In Fig. 3, we show that, using ViT-S/16, SAR can largely speed-up training. For instance, ViT-S/16 + SAR, with 100 epochs, achieves almost the same accuracy as the baseline trained with 150 epochs, while we surpass the final baseline accuracy (79.8% at epoch 300) with only 250 training epochs (79.9% at epoch 250).

**Training from scratch on small-medium datasets.** Comparing the improvement obtained using ViT-S/16 + SAR on IN-1K (+0.9) with the corresponding improvement obtained on IN-100 (+4.42, Tab. 1 (c)), we observe that SAR is relatively more effective when the dataset size is smaller. This is likely due to the fact that, usually, regularization techniques are most effective with small(er) datasets [48, 5]. For instance, Balestrieri *et al.* [5] empirically show that common data-augmentation techniques are more relatively effective with a smaller training dataset, which is quite intuitive, being data-augmentation used to *increase the diversity* of a dataset. Similarly, SAR extracts information

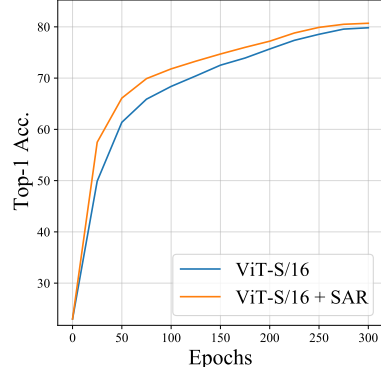


Figure 3: IN-1K, validation set accuracy with respect to the number of training epochs.

from images using a self-supervised pretext task based on our proposed spatial entropy loss (§1), and this additional supervision signal is relatively more effective when there is less supervision data. To further validate this empirical observation, we present another set of experiments in which we follow a recent trend of works [48, 26, 10] where VTs are trained from scratch on small-medium datasets (without pre-training on IN-1K). Specifically, we strictly follow the training protocol proposed in [26], where 5,000 epochs are used to train ViT-S/16 directly on each target dataset. The results are shown in Tab. 3, where the accuracy values of the baseline (ViT-S/16 without SAR) are reported from [26]. Tab. 3 shows that SAR can drastically improve the ViT-S/16 accuracy on these small-medium datasets, with a relative improvement ranging in  $[+18.71, +29.35]$ .

**Transfer learning.** In this battery of experiments, we evaluate SAR in a transfer learning scenario. We adopt the four datasets used in [24, 66, 19, 14]: CIFAR-10 and CIFAR-100 [45], Oxford Flowers102 [55], and Oxford-IIIT-Pets [56]. The standard transfer learning protocol consists in pre-training on IN-1K, and then fine-tuning on each dataset. This corresponds to the first row in Tab. 4, where the IN-1K pre-trained model is ViT-S/16 in Tab. 2. The next three rows show different pre-training/fine-tuning configurations, in which we use SAR in one of the two phases or in both (see the Supplementary for more details). All the configurations lead to an overall improvement of the accuracy with respect to the baseline, and show that SAR can be flexibly used. For instance, SAR can be used when fine-tuning a VT trained in a standard way, without the need to re-train it on ImageNet.

**Robustness with respect to out-of-distribution testing.** Finally, we follow [4] to test the robustness of our VTs trained with SAR when the testing distribution is different from the training distribution. Specifically, Bai *et al.* [4] select two different testing set: (1) ImageNet-A [37], which are real-world images but collected from challenging scenarios (e.g., occlusions, fog scenes, etc.), and (2) ImageNet-C [36], which is designed to measure a model robustness against common image corruptions. Note that training is performed on IN-1K. Thus, in Tab. 5, ViT-S/16 and ViT-S/16 + SAR correspond to the models we trained on IN-1K whose results on the IN-1K standard validation set are reported in Tab. 2. ImageNet-A and ImageNet-C are used *only for testing*, thus they are useful to assess the behaviour of a model when evaluated on a distribution different from the training distribution [4]. The results reported in Tab. 5 show that SAR can drastically improve the robustness of ViT (note that with the mCE metric, the lower is better [4]). We presume that this is a side-effect of our spatial entropy loss minimization, which leads to heads usually focusing on the foreground objects and, hence, reducing the dependence with respect to the background appearance variability distribution. In the next section, we analyze this aspect more in-depth.

### 5.3 Attention map analysis

This section qualitatively and quantitatively analyses the attention maps obtained using SAR. Fig. 4 visually compares the attention maps obtained with ViT-S/16 and ViT-S/16 + SAR. As expected, standard training generates attention maps with a widely spread structure. Conversely, using SAR, a semantic segmentation structure clearly emerges. Note that, similarly to the self-supervised results

Table 2: IN-1K experiments with different VTs. For each tested VT, we plugged SAR on the publicly available code of the corresponding baseline and we used the suggested hyperparameter values for training. All results but ours are reported from the corresponding paper indicated in the column ‘‘Training Protocol’’. All the results have been obtained using 300 training epochs.

Architecture	Training Protocol	Params (M)	FLOPs (G)	Top-1 Acc.
ViT-T/16	DEiT [66]	5	1.6	72.2
ViT-T/16 + SAR	DEiT	5	1.6	<b>72.4 (+0.2)</b>
ViT-S/16	DEiT [66]	22	4.7	79.8
ViT-S/16 + SAR	DEiT	22	4.7	<b>80.7 (+0.9)</b>
T2T-ViT-14	T2T [77]	21.5	6.1	81.5
T2T-ViT-14 + SAR	T2T	21.5	6.1	<b>81.9 (+0.4)</b>
PVT-Small	PVT [71]	24.5	3.8	79.8
PVT-Small + SAR	PVT	24.5	3.8	79.84 (+0.04)
CvT-13	CvT [73]	20	4.5	81.6
CvT-13 + SAR	CvT	20	4.5	<b>81.8 (+0.2)</b>

Table 3: Training from scratch on small-medium datasets.

Model	Cars	Clipart	Painting	Sketch
ViT-S/16	35.3	41.0	38.4	37.2
ViT-S/16+SAR	<b>64.65</b> (+29.35)	<b>64.95</b> (+23.95)	<b>57.11</b> (+18.17)	<b>62.98</b> (+30.78)

Table 4: Transfer learning results on different datasets (100 epochs fine-tuning). The first row corresponds to a standard fine-tuning protocol, while the other configurations include SAR either in the pre-training or in the fine-tuning stage.

SAR pre-training	SAR fine-tuning	CIFAR-10	CIFAR-100	Flowers	Pets
✗	✗	98.59	88.95	95.07	92.21
✓	✗	98.69 (+0.1)	89.19 (+0.24)	96.05 (+0.98)	92.7 (+0.49)
✗	✓	98.72 (+0.13)	88.95	95.1 (+0.03)	92.34 (+0.13)
✓	✓	98.65 (+0.06)	89.21 (+0.26)	96.1 (+1.03)	92.7 (+0.49)

shown in DINO [14], these segmentation masks have been obtained *without any pixel-level annotation*. However, differently from [14], we have *explicitly* encouraged the network to produce attention maps with low spatial entropy. For a quantitative analysis, we follow the protocol used in [14, 53], where the Jaccard similarity is used to compare the ground-truth segmentation masks of the objects in PASCAL VOC-12 [28] with the thresholded attention masks of the last ViT block. Specifically, the attention maps of all the heads are thresholded to keep 60% of the mass, and the head with the highest Jaccard similarity with the ground-truth is selected [14, 53]. Tab. 6 shows that SAR significantly improves the segmentation results, quantitatively confirming the qualitative analysis in Fig. 4.

Figure 4: A qualitative comparison between the attention maps generated by ViT-S/16 (left) and ViT-S/16 + SAR (right). For each image, we show all the 6 attention maps ( $A^h$ ) corresponding to the 6 last-block heads, computed using only the [CLS] token query.

## 6 Conclusions

In this paper we proposed SAR, a VT training regularization method which is based on a new spatial entropy loss. Specifically, the proposed loss is based on the intuitive idea that objects usually correspond to connected regions, and thus it penalizes spatially disordered attention maps. In this way, we can extract additional self-supervised information from the training images, which acts as a regularization and it is specifically helpful when training on small-medium datasets. Moreover, we also proposed to remove the last-block MSA skip connections and LN layers, a minor architectural change which prevents the propagation of the patch-token representations through the identity path. We empirically showed that this removal is beneficial, with and without our spatial entropy loss.

SAR can be very easily plugged into the most common VT architectures, and our experiments show that this training regularization can boost the classification accuracy and speed-up training, independently of the specific VT and without architecture or task-specific hyperparameter tuning.

**Limitations.** Since training VTs is very computationally expensive, in our experiments we used only small/medium capacity VTs. We leave the extension of our empirical analysis to larger capacity

Table 5: Out-of-distribution testing robustness on ImageNet-A (IN-A) and ImageNet-C (IN-C).

Model	IN-A (Acc. $\uparrow$ )	IN-C (mCE $\downarrow$ )
ViT-S/16	19.2	52.8
ViT-S/16 + SAR	<b>22.39</b> (+3.19)	<b>51.6</b> (-1.2)

Table 6: A comparison of the segmentation properties of the attention maps on PASCAL VOC-12.

Model	Jaccard similarity ( $\uparrow$ )
ViT-S/16	19.18
ViT-S/16 + SAR	<b>31.19</b> (+12.01)

VTs for the future. For the same computational reasons, we have not tuned hyperparameters on the datasets. However, we believe that the SAR accuracy improvement, obtained in all the tested scenarios without hyperparameter tuning, further shows its robustness and ease to use.

## References

- [1] Linda Altieri, Daniela Cocchi, and Giulia Roli. SpatEntropy: Spatial Entropy Measures in R. *arXiv:1804.05521*, 2018.
- [2] Yuki Markus Asano, Christian Rupprecht, and Andrea Vedaldi. Self-labelling via simultaneous clustering and representation learning. In *ICLR*, 2020.
- [3] Roman Bachmann, David Mizrahi, Andrei Atanov, and Amir Zamir. MultiMAE: Multi-modal Multi-task Masked Autoencoders. *arXiv:2204.01678*, 2022.
- [4] Yutong Bai, Jieru Mei, Alan L. Yuille, and Cihang Xie. Are transformers more robust than cnns? In *NeurIPS*, 2021.
- [5] Randall Balestrieri, Leon Bottou, and Yann LeCun. The effects of regularization and data augmentation are class dependent. *arXiv:2204.03632*, 2022.
- [6] Hangbo Bao, Li Dong, and Furu Wei. BEiT: BERT pre-training of image transformers. *arXiv:2106.08254*, 2021.
- [7] Adrien Bardes, Jean Ponce, and Yann LeCun. VICReg: Variance-invariance-covariance regularization for self-supervised learning. *arXiv:2105.04906*, 2021.
- [8] Michael Batty. Spatial entropy. *Geographical analysis*, 6(1):1–31, 1974.
- [9] Miguel A Bautista, Artsiom Sanakoyeu, Ekaterina Tikhoncheva, and Bjorn Ommer. CliqueCNN: deep unsupervised exemplar learning. In *NeurIPS*, 2016.
- [10] Yun-Hao Cao and Jianxin Wu. Rethinking self-supervised learning: Small is beautiful. *arXiv:2103.13559*, 2021.
- [11] Nicolas Carion, Francisco Massa, Gabriel Synnaeve, Nicolas Usunier, Alexander Kirillov, and Sergey Zagoruyko. End-to-end object detection with transformers. In *ECCV*, 2020.
- [12] Mathilde Caron, Piotr Bojanowski, Armand Joulin, and Matthijs Douze. Deep clustering for unsupervised learning of visual features. In *ECCV*, 2018.
- [13] Mathilde Caron, Ishan Misra, Julien Mairal, Priya Goyal, Piotr Bojanowski, and Armand Joulin. Unsupervised learning of visual features by contrasting cluster assignments. In *NeurIPS*, 2020.
- [14] Mathilde Caron, Hugo Touvron, Ishan Misra, Hervé Jégou, Julien Mairal, Piotr Bojanowski, and Armand Joulin. Emerging properties in self-supervised vision transformers. *arXiv:2104.14294*, 2021.
- [15] Mark Chen, Alec Radford, Rewon Child, Jeffrey Wu, Heewoo Jun, David Luan, and Ilya Sutskever. Generative pretraining from pixels. In *ICML*, 2020.
- [16] Ting Chen, Simon Kornblith, Mohammad Norouzi, and Geoffrey E. Hinton. A simple framework for contrastive learning of visual representations. In *ICML*, 2020.
- [17] Xiaokang Chen, Mingyu Ding, Xiaodi Wang, Ying Xin, Shentong Mo, Yunhao Wang, Shumin Han, Ping Luo, Gang Zeng, and Jingdong Wang. Context autoencoder for self-supervised representation learning. *arXiv:2202.03026*, 2022.
- [18] Xinlei Chen and Kaiming He. Exploring simple siamese representation learning. In *CVPR*, 2021.

- [19] Xinlei Chen, Saining Xie, and Kaiming He. An empirical study of training self-supervised vision transformers. *ICCV*, 2021.
- [20] Zhigang Dai, Bolun Cai, Yugeng Lin, and Junying Chen. UP-DETR: unsupervised pre-training for object detection with transformers. In *CVPR*, 2021.
- [21] Stéphane d’Ascoli, Hugo Touvron, Matthew L. Leavitt, Ari S. Morcos, Giulio Biroli, and Levent Sagun. ConViT: Improving vision transformers with soft convolutional inductive biases. In *ICML*, 2021.
- [22] Jacob Devlin, Ming-Wei Chang, Kenton Lee, and Kristina Toutanova. BERT: Pre-training of deep bidirectional transformers for language understanding. In *NAACL*, 2019.
- [23] Xiaoyi Dong, Jianmin Bao, Ting Zhang, Dongdong Chen, Weiming Zhang, Lu Yuan, Dong Chen, Fang Wen, and Nenghai Yu. PeCo: Perceptual Codebook for BERT Pre-training of Vision Transformers. *arXiv:2111.12710*, 2021.
- [24] Alexey Dosovitskiy, Lucas Beyer, Alexander Kolesnikov, Dirk Weissenborn, Xiaohua Zhai, Thomas Unterthiner, Mostafa Dehghani, Matthias Minderer, Georg Heigold, Sylvain Gelly, Jakob Uszkoreit, and Neil Houlsby. An image is worth 16x16 words: Transformers for image recognition at scale. In *ICLR*, 2021.
- [25] Debidatta Dwibedi, Yusuf Aytar, Jonathan Tompson, Pierre Sermanet, and Andrew Zisserman. With a little help from my friends: Nearest-neighbor contrastive learning of visual representations. In *ICCV*, 2021.
- [26] Alaaeldin El-Nouby, Gautier Izacard, Hugo Touvron, Ivan Laptev, Hervé Jégou, and Edouard Grave. Are large-scale datasets necessary for self-supervised pre-training? *arXiv:2112.10740*, 2021.
- [27] Aleksandr Ermolov, Aliaksandr Siarohin, Enver Sangineto, and Nicu Sebe. Whitening for self-supervised representation learning. In *ICML*, 2021.
- [28] Mark Everingham, Luc Van Gool, Christopher K. I. Williams, John M. Winn, and Andrew Zisserman. The pascal visual object classes (VOC) challenge. *Int. J. Comput. Vis.*, 88(2):303–338, 2010.
- [29] Wouter Van Gansbeke, Simon Vandenhende, Stamatios Georgoulis, Marc Proesmans, and Luc Van Gool. SCAN: learning to classify images without labels. In *ECCV*, 2020.
- [30] Costantino Grana, Daniele Borghesani, and Rita Cucchiara. Optimized block-based connected components labeling with decision trees. *IEEE Trans. Image Process.*, 19(6):1596–1609, 2010.
- [31] Jean-Bastien Grill, Florian Strub, Florent Altché, Corentin Tallec, Pierre H. Richemond, Elena Buchatskaya, Carl Doersch, Bernardo Avila Pires, Zhaohan Daniel Guo, Mohammad Gheshlaghi Azar, Bilal Piot, Koray Kavukcuoglu, Rémi Munos, and Michal Valko. Bootstrap your own latent: A new approach to self-supervised learning. In *NeurIPS*, 2020.
- [32] Meng-Hao Guo, Junxiong Cai, Zheng-Ning Liu, Tai-Jiang Mu, Ralph R. Martin, and Shi-Min Hu. PCT: Point cloud transformer. *Comput. Vis. Media*, 7(2):187–199, 2021.
- [33] Kaiming He, Xinlei Chen, Saining Xie, Yanghao Li, Piotr Dollár, and Ross B. Girshick. Masked autoencoders are scalable vision learners. *arXiv:2111.06377*, 2021.
- [34] Kaiming He, Haoqi Fan, Yuxin Wu, Saining Xie, and Ross Girshick. Momentum contrast for unsupervised visual representation learning. In *CVPR*, 2020.
- [35] Kaiming He, Xiangyu Zhang, Shaoqing Ren, and Jian Sun. Deep residual learning for image recognition. In *CVPR*, 2016.
- [36] Dan Hendrycks and Thomas G. Dietterich. Benchmarking neural network robustness to common corruptions and perturbations. In *ICLR*, 2018.
- [37] Dan Hendrycks, Kevin Zhao, Steven Basart, Jacob Steinhardt, and Dawn Song. Natural adversarial examples. In *CVPR*, 2019.
- [38] R. Devon Hjelm, Alex Fedorov, Samuel Lavoie-Marchildon, Karan Grewal, Philip Bachman, Adam Trischler, and Yoshua Bengio. Learning deep representations by mutual information estimation and maximization. In *ICLR*, 2019.
- [39] Tianyu Hua, Yonglong Tian, Sucheng Ren, Hang Zhao, and Leonid Sigal. Self-supervision through Random Segments with Autoregressive Coding (RandSAC). *arXiv:2203.12054*, 2022.

[40] Tianyu Hua, Wenxiao Wang, Zihui Xue, Yue Wang, Sucheng Ren, and Hang Zhao. On feature decorrelation in self-supervised learning. *arXiv:2105.00470*, 2021.

[41] Drew A. Hudson and C. Lawrence Zitnick. Generative Adversarial Transformers. In *ICML*, 2021.

[42] Xu Ji, João F. Henriques, and Andrea Vedaldi. Invariant information clustering for unsupervised image classification and segmentation. In *ICCV*, 2019.

[43] Yifan Jiang, Shiyu Chang, and Zhangyang Wang. TransGAN: Two transformers can make one strong GAN. *arXiv:2102.07074*, 2021.

[44] Ioannis Kakogeorgiou, Spyros Gidaris, Bill Psomas, Yannis Avrithis, Andrei Bursuc, Konstantinos Karantzalos, and Nikos Komodakis. What to Hide from Your Students: Attention-Guided Masked Image Modeling. *arXiv:2203.12719*, 2022.

[45] Alex Krizhevsky, Geoffrey Hinton, et al. Learning multiple layers of features from tiny images. 2009.

[46] Yanghao Li, Chao-Yuan Wu, Haoqi Fan, Karttikeya Mangalam, Bo Xiong, Jitendra Malik, and Christoph Feichtenhofer. Improved multiscale vision transformers for classification and detection. *arXiv:2112.01526*, 2021.

[47] Yawei Li, Kai Zhang, Jie Zhang Cao, Radu Timofte, and Luc Van Gool. LocalViT: Bringing locality to vision transformers. *arXiv:2104.05707*, 2021.

[48] Yahui Liu, Enver Sangineto, Wei Bi, Nicu Sebe, Bruno Lepri, and Marco De Nadai. Efficient training of visual transformers with small datasets. *NeurIPS*, 2021.

[49] Ze Liu, Yutong Lin, Yue Cao, Han Hu, Yixuan Wei, Zheng Zhang, Stephen Lin, and Baining Guo. Swin transformer: Hierarchical vision transformer using shifted windows. *arXiv:2103.14030*, 2021.

[50] Ilya Loshchilov and Frank Hutter. Decoupled weight decay regularization. In *7th International Conference on Learning Representations, ICLR 2019, New Orleans, LA, USA, May 6-9, 2019*, 2019.

[51] Wenjie Luo, Yujia Li, Raquel Urtasun, and Richard S. Zemel. Understanding the effective receptive field in deep convolutional neural networks. *arXiv:1701.04128*, 2017.

[52] Tim Meinhardt, Alexander Kirillov, Laura Leal-Taixé, and Christoph Feichtenhofer. TrackFormer: Multi-object tracking with transformers. *arXiv:2101.02702*, 2021.

[53] Muzammal Naseer, Kanchana Ranasinghe, Salman H. Khan, Munawar Hayat, Fahad Shahbaz Khan, and Ming-Hsuan Yang. Intriguing properties of vision transformers. *arXiv:2105.10497*, 2021.

[54] Daniel Neimark, Omri Bar, Maya Zohar, and Dotan Asselmann. Video transformer network. *arXiv:2102.00719*, 2021.

[55] Maria-Elena Nilsback and Andrew Zisserman. Automated flower classification over a large number of classes. In *Indian Conference on Computer Vision, Graphics & Image Processing*, 2008.

[56] Omkar M. Parkhi, Andrea Vedaldi, Andrew Zisserman, and C. V. Jawahar. Cats and dogs. In *CVPR*, 2012.

[57] Alec Radford and Karthik Narasimhan. Improving language understanding by generative pre-training. 2018.

[58] Maithra Raghu, Thomas Unterthiner, Simon Kornblith, Chiyuan Zhang, and Alexey Dosovitskiy. Do vision transformers see like convolutional neural networks? *arXiv:2108.08810*, 2021.

[59] Aditya Ramesh, Mikhail Pavlov, Gabriel Goh, Scott Gray, Chelsea Voss, Alec Radford, Mark Chen, and Ilya Sutskever. Zero-shot text-to-image generation. In *ICML*, 2021.

[60] Yongming Rao, Wenliang Zhao, Guangyi Chen, Yansong Tang, Zheng Zhu, Guan Huang, Jie Zhou, and Jiwen Lu. DenseCLIP: Language-guided dense prediction with context-aware prompting. *arXiv:2112.01518*, 2021.

[61] Q.R. Razlighi and Nasser Kehtarnavaz. A comparison study of image spatial entropy. In *Electronic Imaging*, 2009.

[62] Leonid I. Rudin, Stanley Osher, and Emad Fatemi. Nonlinear total variation based noise removal algorithms. *Physica D: Nonlinear Phenomena*, 60(1):259–268, 1992.

[63] Olga Russakovsky, Jia Deng, Hao Su, Jonathan Krause, Sanjeev Satheesh, Sean Ma, Zhiheng Huang, Andrej Karpathy, Aditya Khosla, Michael Bernstein, et al. Imagenet large scale visual recognition challenge. *International Journal of Computer Vision*, 115(3):211–252, 2015.

[64] Robin Strudel, Ricardo Garcia, Ivan Laptev, and Cordelia Schmid. Segmenter: Transformer for semantic segmentation. In *ICCV*, 2021.

[65] Yonglong Tian, Dilip Krishnan, and Phillip Isola. Contrastive multiview coding. In *ECCV*, 2020.

[66] Hugo Touvron, Matthieu Cord, Matthijs Douze, Francisco Massa, Alexandre Sablayrolles, and Hervé Jégou. Training data-efficient image transformers & distillation through attention. *arXiv:2012.12877*, 2020.

[67] F. Tupin, M. Sigelle, and H. Maitre. Definition of a spatial entropy and its use for texture discrimination. In *ICIP*, 2000.

[68] Aäron van den Oord, Yazhe Li, and Oriol Vinyals. Representation learning with contrastive predictive coding. *arXiv:1807.03748*, 2018.

[69] Ashish Vaswani, Noam Shazeer, Niki Parmar, Jakob Uszkoreit, Llion Jones, Aidan N. Gomez, Łukasz Kaiser, and Illia Polosukhin. Attention is all you need. In *NeurIPS*, 2017.

[70] Tongzhou Wang and Phillip Isola. Understanding contrastive representation learning through alignment and uniformity on the hypersphere. In *ICML*, 2020.

[71] Wenhui Wang, Enze Xie, Xiang Li, Deng-Ping Fan, Kaitao Song, Ding Liang, Tong Lu, Ping Luo, and Ling Shao. Pyramid vision transformer: A versatile backbone for dense prediction without convolutions. In *ICCV*, 2021.

[72] Chen Wei, Haoqi Fan, Saining Xie, Chao-Yuan Wu, Alan L. Yuille, and Christoph Feichtenhofer. Masked feature prediction for self-supervised visual pre-training. *arXiv:2112.09133*, 2021.

[73] Haiping Wu, Bin Xiao, Noel Codella, Mengchen Liu, Xiyang Dai, Lu Yuan, and Lei Zhang. CvT: Introducing convolutions to vision transformers. *arXiv:2103.15808*, 2021.

[74] Zhenda Xie, Zheng Zhang, Yue Cao, Yutong Lin, Jianmin Bao, Zhuliang Yao, Qi Dai, and Han Hu. SimMIM: A simple framework for masked image modeling. *arXiv:2111.09886*, 2021.

[75] Weijian Xu, Yifan Xu, Tyler Chang, and Zhuowen Tu. Co-scale conv-attentional image transformers. *arXiv:2104.06399*, 2021.

[76] Kun Yuan, Shaopeng Guo, Ziwei Liu, Aojun Zhou, Fengwei Yu, and Wei Wu. Incorporating convolution designs into visual transformers. *arXiv:2103.11816*, 2021.

[77] Li Yuan, Yunpeng Chen, Tao Wang, Weihao Yu, Yujun Shi, Zihang Jiang, Francis EH Tay, Jiashi Feng, and Shuicheng Yan. Tokens-to-token ViT: Training vision transformers from scratch on ImageNet. In *ICCV*, 2021.

[78] Jure Zbontar, Li Jing, Ishan Misra, Yann LeCun, and Stéphane Deny. Barlow twins: Self-supervised learning via redundancy reduction. In *ICML*, 2021.

[79] Hengshuang Zhao, Li Jiang, Jiaya Jia, Philip H. S. Torr, and Vladlen Koltun. Point transformer. *arXiv:2012.09164*, 2020.

[80] Ce Zheng, Sijie Zhu, Matias Mendieta, Taojiannan Yang, Chen Chen, and Zhengming Ding. 3D Human pose estimation with spatial and temporal transformers. *ICCV*, 2021.

[81] Jinghao Zhou, Chen Wei, Huiyu Wang, Wei Shen, Cihang Xie, Alan L. Yuille, and Tao Kong. iBOT: Image BERT Pre-Training with Online Tokenizer. *arXiv:2111.07832*, 2021.

[82] Xizhou Zhu, Weijie Su, Lewei Lu, Bin Li, Xiaogang Wang, and Jifeng Dai. Deformable DETR: Deformable transformers for end-to-end object detection. In *ICLR*, 2021.

[83] Chengxu Zhuang, Alex Lin Zhai, and Daniel Yamins. Local aggregation for unsupervised learning of visual embeddings. In *ICCV*, 2019.

## A Pseudo-code of the Spatial Entropy loss

Fig. 5 shows the pseudo-code for  $\mathcal{L}_{se}$  (Eq. (9) of the main paper). The goal is twofold: to show how easy is to compute  $\mathcal{L}_{se}$ , and how to make it differentiable. Specifically, Eq. (6) of the main paper is based on a connected component algorithm which is not differentiable. However, once  $C^h$  is computed, each element  $C_j \in C^h$  ( $C_j = \{(x_1, y_1), \dots, (x_{n_j}, y_{n_j})\}$ ) can be represented as a binary mask  $M_j$ , defined as:

$$M_j[x, y] = \begin{cases} 1, & \text{if } (x, y) \in C_j \\ 0 & \text{otherwise} \end{cases} \quad (12)$$

Using Eq. (12), it is possible to compute the probability  $P^h(C_j)$  of the component  $C_j$  using matrix multiplication, which is done efficiently on GPUs. In practice, Eq. (8) of the main paper is computed as:

$$P^h(C_j) = \frac{1}{|B^h|} \sum_{(x, y)} B_{x, y}^h \odot M_j[x, y] \quad (13)$$

where  $\odot$  is the element-wise product. This implementation makes it is possible to back-propagate the spatial entropy loss even if the connected component algorithm is not differentiable.

```
# bs      : batch size
# H      : number of heads
# k x k : size of the embedding grid
# S      : defined in Eq. 4 (main paper), tensor with shape [bs, H, k, k]

def SpatialEntropy(S, eps=1e-9):
    bs, H, k, _ = S.size()
    m = torch.mean(S, dim=[2, 3], keepdim=True)
    B = torch.relu(S - m) + eps

    with torch.no_grad():
        batch_idxs, head_idxs, M = connected_components(B)

        p_u = torch.sum(B[batch_idxs, head_idxs] * M, dim=[2, 3])
        p_n = p_u / torch.sum(B, dim=[2, 3])
        SE = -torch.sum((p_n * torch.log(p_n)) / (bs * H))
    return SE
```

Figure 5: PyTorch-like pseudocode for our Spatial Entropy loss.

## B Comparing the spatial entropy loss with other solutions

In our preliminary experiments, we replaced the spatial entropy loss with a different loss based on a *total variation denoising* [62], criterion, which we formulated as:

$$\mathcal{L}_{tv} = \frac{1}{H} \sum_{h=1}^H \sum_{(x, y) \in \{1, \dots, k\}^2} |S_{x, y}^h - S_{x, y+1}^h| + |S_{x, y}^h - S_{x+1, y}^h|. \quad (14)$$

However,  $\mathcal{L}_{tv}$  drastically underperforms  $\mathcal{L}_{se}$  and tends to produce blurred (more uniform) attention maps. The main difference between  $\mathcal{L}_{tv}$  and  $\mathcal{L}_{se}$  is that the thresholding (main paper, Eq. (5)) and the clustering (main paper, Eq. (6)) operations in  $\mathcal{L}_{se}$  group together image regions of variable size and shape which have in common high attention scores for a specific head, and, therefore, they presumably represent the same semantics (e.g., a specific object). In contrast,  $\mathcal{L}_{tv}$  compares patch tokens which are adjacent to each other (e.g.,  $S_{x, y}^h$  and  $S_{x, y+1}^h$ ) but which do not necessarily share the same semantics (e.g.,  $S_{x, y}^h$  may belong to the background while  $S_{x, y+1}^h$  belongs to a foreground object). Thus, the implicit local prior of the two losses is different: in case of  $\mathcal{L}_{se}$ , the local prior is that the image regions corresponding to the highest attention scores (for a specific head) should be spatially grouped in few, big “blobs”, while, in the case of  $\mathcal{L}_{tv}$ , the local prior is that generic adjacent regions should have similar attention scores.

## C Additional experiments

In this section, we present additional experiments following the same setting used in the main paper (e.g., same  $\lambda$  value, using the original VT/algorithm hyperparameters, etc.).

### C.1 Training from scratch on ImageNet-100

In this section, we extend the IN-100 experiments shown in the main paper by including different VT architectures. Tab. 7 shows that SAR improves *all* the tested VTs, consistently with the results on IN-1K (see Tab. 2 of the main paper). Note that the SAR-based improvements on IN-100 are relatively larger than those obtained on IN-1K, confirming that SAR is particularly beneficial with relatively smaller datasets.

Table 7: IN-100 experiments with different VTs. For each tested VT, we plug SAR on the publicly available code of the corresponding baseline and we use the suggested hyperparameter values for training. All the results are obtained using 100 training epochs.

Model	Top-1 Acc.
ViT-S/16 [24]	74.22
ViT-S/16 + SAR	<b>76.72</b> (+2.5)
T2T-ViT-14 [77]	82.42
T2T-ViT-14 + SAR	<b>83.96</b> (+1.54)
PVT-Small [71]	76.57
PVT-Small + SAR	<b>77.78</b> (+1.21)
CvT-13 [73]	83.38
CvT-13 + SAR	<b>85.20</b> (+1.82)

### C.2 Self-supervised experiments on ImageNet-100

In this section, we test SAR in a fully self-supervised scenario. Since self-supervised learning algorithms are very time consuming, we use IN-100, which is a medium-size dataset. We plug SAR on top of two state-of-the-art VT-based self-supervised learning algorithms: MoCo-v3 [19] and DINO [14] (see Sec. 2 of the main paper for a discussion). When we use MoCo-v3, in  $\mathcal{L}_{tot}$  (see Sec. 4.1 in the main paper), we replace the cross-entropy loss ( $\mathcal{L}_{ce}$ ) with the contrastive loss used in [19]. Similarly, when we use DINO, we use as the main task loss the “self-distillation” proposed in [14] and its multi-crop strategy. We used the official code of MoCo-v3 and DINO and we strictly follow the algorithms and the training protocols of the baseline methods, including all the default hyperparameters suggested by the corresponding authors. However, for computational reasons, we used a 1024 batch size for MoCo-v3 and MoCo-v3 + SAR, and a batch size of 512 for DINO and DINO + SAR. The VT backbone is ViT-S/16 for all the methods. More details in Appendix D.

We evaluate all models (with and without SAR) using the standard self-supervised evaluation protocol, consisting in freezing the network after training and then training a linear classifier on top of the frozen features [14, 19]. The results reported in Tab. 8 (a), which shows that, on IN-100, SAR significantly improves these state-of-the-art algorithms, including DINO (which inspired our work).

We qualitatively compare the attention maps obtained with and without SAR in Fig. 6 (MoCo-v3) and Fig. 7 (DINO). Fig. 6 shows that, in MoCo-v3 + SAR, the head-specific attention maps focus on slightly different aspects of the main object, while in MoCo-v3, the attention is much more “disordered” (spread over the whole image). On the other hand, when comparing DINO with DINO + SAR (Fig. 7), the attention map differences are more subtle. However, the higher inter-head variability in DINO + SAR is one interesting difference. For instance, while DINO’s maps usually focus only on the main foreground object, in DINO + SAR, different heads cover different foreground objects (e.g., the cat and the sink in Row 11) or different background regions (e.g., the road and the sky in the “train” figure of Row 5). This difference is probably due to the difference in how DINO and DINO + SAR are optimized. In fact, in DINO, the only source of supervision is the comparison between two different views of the same image (see Sec. 2 of the main paper), which likely encourages the

Table 8: Quantitative results of self-supervised models trained on IN-100 for 300 epochs. (a) Accuracy on IN-100 evaluated through linear probing. (b) Segmentation properties of the attention maps on PASCAL VOC-12.

Method	Top-1 Acc.	Method	Jaccard similarity
MoCo-v3 [19]	77.60	MoCo-v3 [19]	27.40
MoCo-v3 + SAR	<b>78.88</b> (+1.28)	MoCo-v3 + SAR	<b>33.10</b> (+6.17)
DINO [14]	77.42	DINO [14]	35.06
DINO + SAR	<b>79.90</b> (+2.48)	DINO + SAR	<b>35.28</b> (+0.22)

(a)

(b)

Table 11: Quantitative results on ViT-S/16 trained with and without SAR and compared with [48]. All models are trained in ImageNet-1K for 300 epochs.

Method	Top-1 Acc.
ViT-S/16 [24]	79.8
ViT-S/16 + DRLoc [48]	80.2 (+0.4)
ViT-S/16 + SAR	<b>80.7</b> (+0.9)

network to focus on the objects most frequently in common. On the other hand, in DINO + SAR, the creation of connected regions is also encouraged inside each image view employing  $\mathcal{L}_{se}$ .

Overall, the qualitative observations are confirmed by the quantitative results in Tab. 8 (b), where we follow the protocol described in Sec. 5.3 of the main paper. SAR increases the Jaccard similarity of both self-supervised algorithms.

### C.3 Supervised case, additional experiments on ImageNet-1K

In this section, we extend the analysis of Sec. 5.3 (main paper) providing additional qualitative and quantitative results obtained using supervised training.

Fig. 8 shows the attention maps of ViT-S/16 and ViT-S/16 + SAR. These attention maps show that the ViT-S/16 attention scores are spread over all the image, while in ViT-S/16 + SAR they are much more spatially clustered and usually focused on the main object(s) of the input image. For example, the first row shows that the heads of ViT-S/16 focus on the upper part of the image, and only the keyboard of the laptop emerges. Vice versa, from the ViT-S/16 + SAR attention heads, it is possible to recognise the shape and size of the laptop precisely. Similarly, the second last row shows an example where the input image contains some elephants. While the different heads of ViT-S/16 seem to focus mainly on the background, the first head of ViT-S/16 + SAR is clearly focused on the elephants. Importantly, different heads of ViT-S/16 + SAR usually focus on different semantic concepts, which shows that there are no collapse phenomena using the spatial entropy loss (see Eq. (7) of the main paper and the corresponding discussion in Sec. 4.3).

Finally, we compare SAR with the Dense Relative Localization (DRLoc) loss [48], which is based on an auxiliary self-supervised task used to regularize VT training when training data is scarce. DRLoc encourages the VT to learn spatial relations within an image by predicting the relative distance between the  $(x, y)$  positions of randomly sampled output embeddings from the  $k \times k$  grid of the last layer  $L$ . Table 11 shows that SAR outperforms DRLoc [48], using the same training protocol and a ViT-S/16 architecture trained on ImageNet-1K.

## D Implementation details

In the following, we list the implementation details not mentioned in the main paper. Unless stated otherwise, we train our models on 8 V100 GPUs.

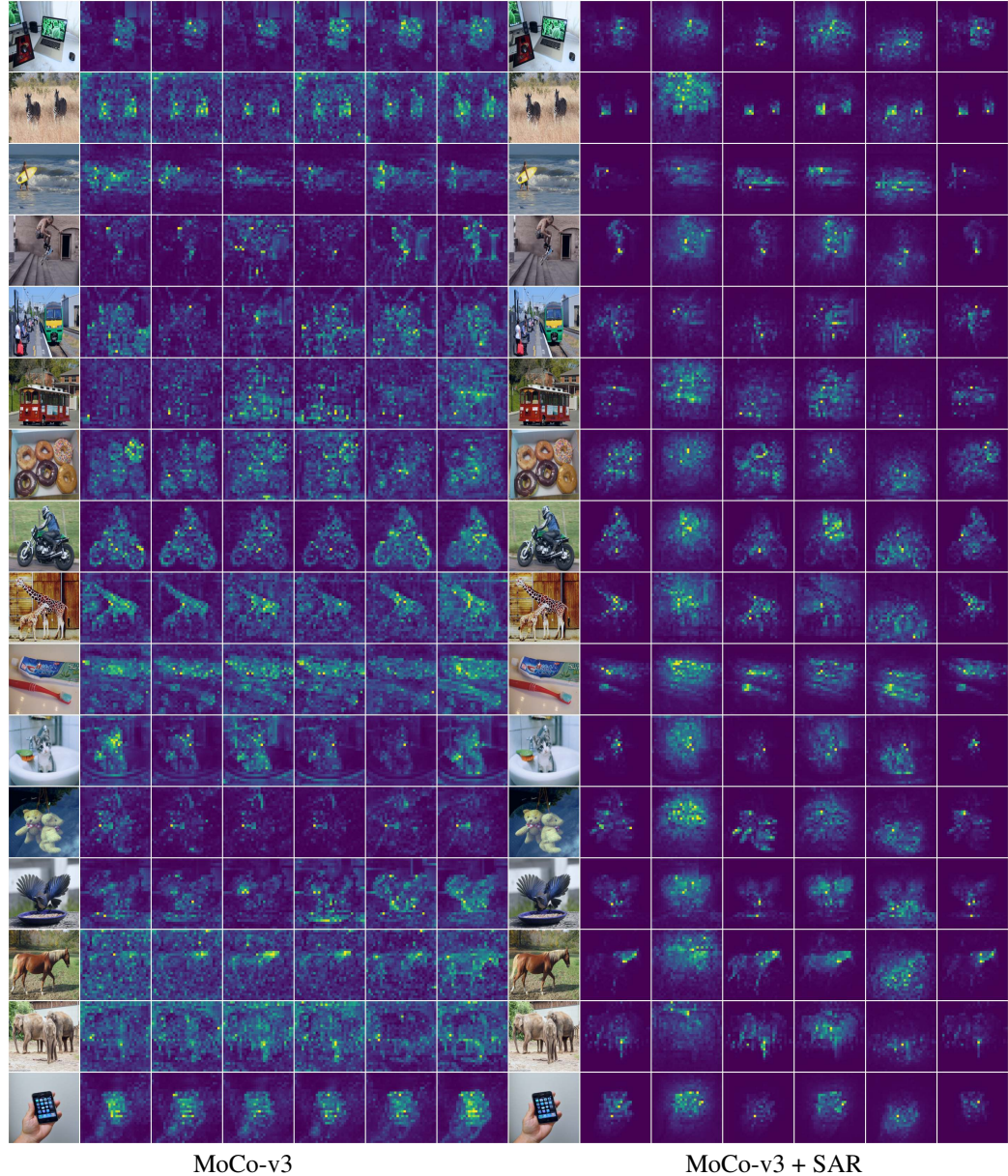


Figure 6: A qualitative comparison between the attention maps generated by MoCo-v3 and MoCo-v3 + SAR with the ViT-S/16 backbone (training on IN-100). For each image, we show all the 6 attention maps ( $A^h$ ) corresponding to the 6 last-block heads, computed using only the [CLS] token query.

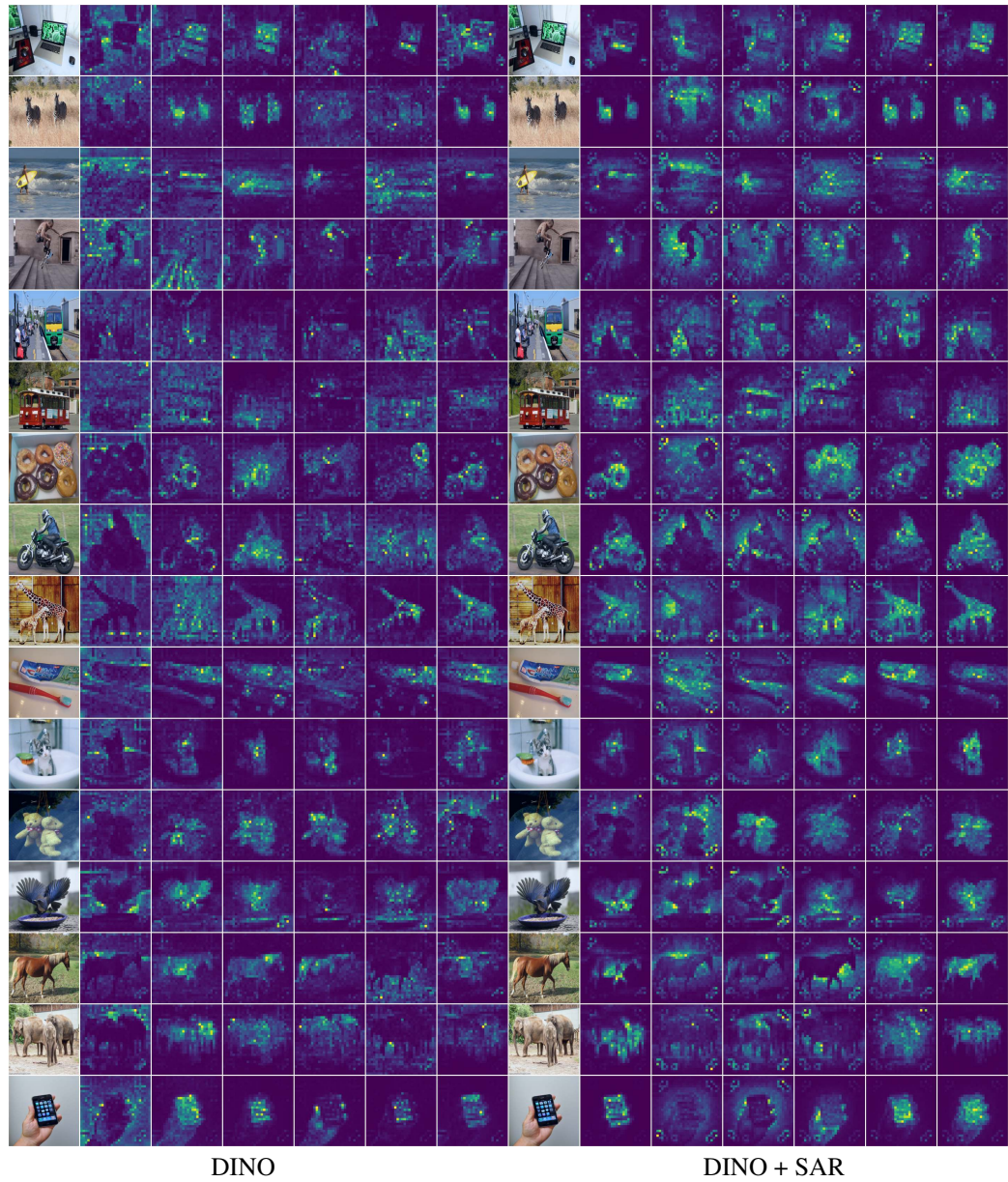


Figure 7: A qualitative comparison between the attention maps generated by DINO and DINO + SAR with the ViT-S/16 backbone (training on IN-100).

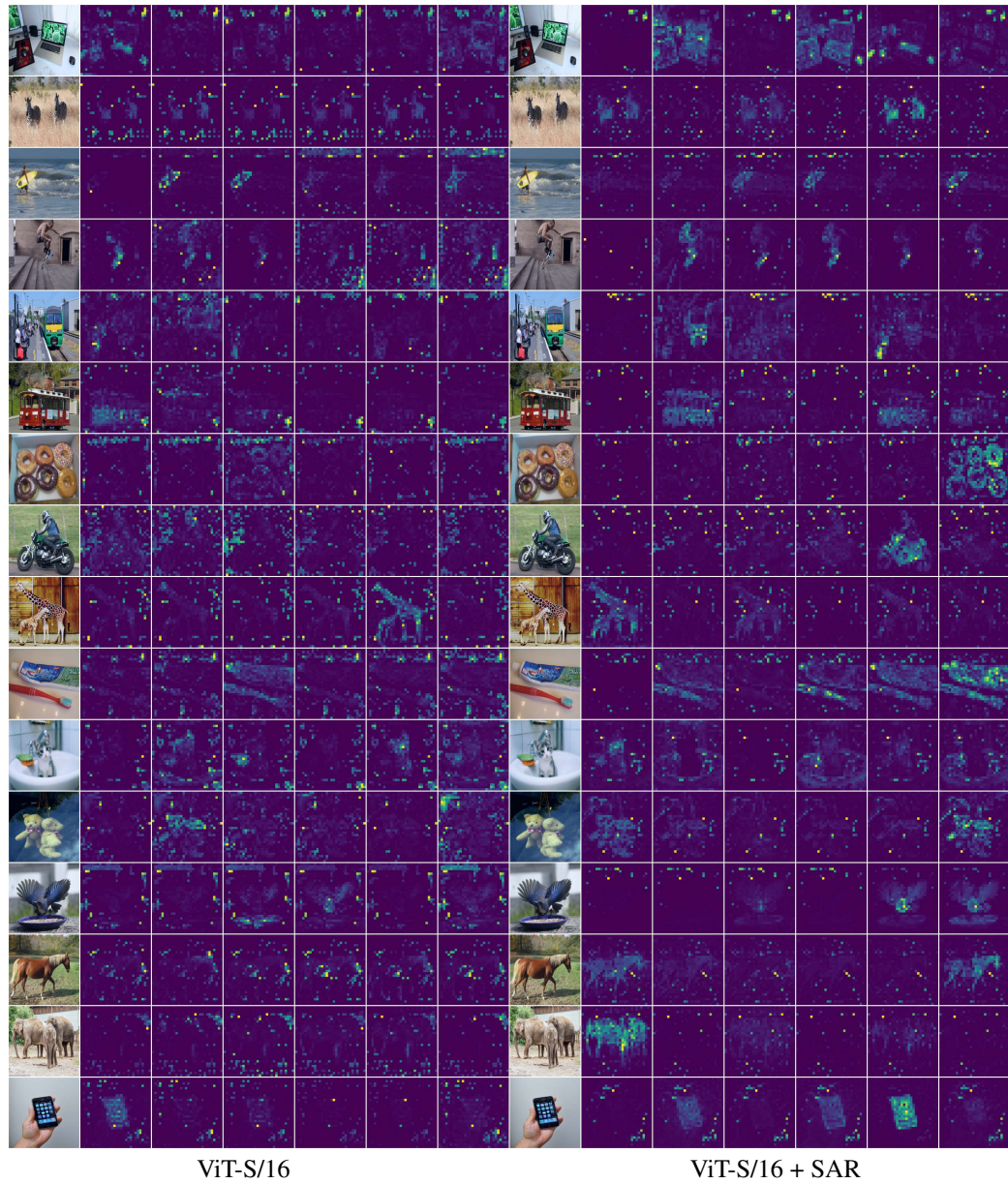


Figure 8: A qualitative comparison between the attention maps generated by ViT-S/16 and ViT-S/16 + SAR (supervised case, training on IN-1K).

## D.1 ViT based models

We train our models using the public code of [66]<sup>2</sup> for ViT and we modify the original code when we use SAR, as described in Sec. 4.2 of the main paper. The models are trained with a batch size of 1024, using the AdamW [50] optimizer with initial learning rate of 0.001, a cosine learning rate schedule, a weight decay of 0.05 and using the original data-augmentation protocol.

## D.2 Hybrid architectures

In all the supervised experiments, we used the officially released code for PVT [71]<sup>3</sup>, T2T [77]<sup>4</sup> and CvT [73]<sup>5</sup>, strictly following the original training protocol for each architecture.

PVT and T2T are trained with batch size of 1024, using the AdamW optimizer with an initial learning rate of 0.001, momentum 0.9 and weight decay of 0.05. CvT [73] is trained with a batch size of 2048 and an initial learning rate of 0.02, decayed with a cosine schedule. The data augmentations of the original papers are based on the DeiT protocol [66]. We refer the reader to the original papers for further details. When we use SAR, we modify the original public code, following Sec. 4.2 of the main paper.

## D.3 Fine-tuning

We fine-tune ViT-S/16 models pretrained on IN-1K (see Tab. 2 of the main paper), always keeping unchanged the VT architecture used in the pre-training stage. This is done to avoid making the adaptation task more difficult, since each of the four datasets used in Tab. 4 is composed of a relatively small number of samples. For instance, when SAR is used during pre-training and removed during fine-tuning (second row of Tab. 4), in the fine-tuning stage we use only  $\mathcal{L}_{ce}$  for training but we do *not* re-introduce skip connections or LN layers in the last block (i.e., we use Eq. (10)-Eq. (11) of the main paper when fine-tuning). Conversely, when the pre-training is performed without SAR which is introduced only in the fine-tuning stage (third row of Tab. 4), when fine-tuning, we use  $\mathcal{L}_{tot} = \mathcal{L}_{ce} + \lambda \mathcal{L}_{se}$ , but keeping the standard skip connections and the LN layer in the last block (Eq. (1)-Eq. (2) of the main paper).

The models are fine-tuned for 100 epochs with a batch size of 512, and an initial learning rate of 0.0005 decayed with a cosine schedule.

## D.4 Self-supervised experiments

In our self-supervised experiments, we adopt the original code for MoCo-v3 [19]<sup>6</sup> and DINO [14]<sup>7</sup> with a ViT-S/16 backbone. For computational reasons, we restrict our experiments training the models on IN-100 for 300 epochs. Moreover, to fit the available resources, we reduce the batch size to 1024 for MoCo-v3 while DINO is trained with the default multi-crop strategy ( $2 \times 224^2 + 10 \times 96^2$ ), but with a batch size of 512. We thoroughly follow the authors' specifications for the other hyperparameters. The results in Tab. 8 are obtained using a standard linear evaluation protocol in which the pretrained backbone is frozen, and a linear classifier is trained on top of it, with SGD for 100 epochs on IN-100.

## E Dataset licensing details

CIFAR-10, CIFAR-100 are released to the public with a non-commercial research and/or educational use<sup>8</sup>. Oxford flower102 is released to the public with an unknown license through its website<sup>9</sup>,

<sup>2</sup><https://github.com/facebookresearch/deit>

<sup>3</sup><https://github.com/whai362/PVT/tree/v1>

<sup>4</sup><https://github.com/yitu-opensource/T2T-ViT>

<sup>5</sup><https://github.com/microsoft/CvT>

<sup>6</sup><https://github.com/facebookresearch/moco-v3>

<sup>7</sup><https://github.com/facebookresearch/dino>

<sup>8</sup><https://www.cs.toronto.edu/~kriz/cifar.html>

<sup>9</sup><https://www.roberts.ox.ac.uk/~vgg/data/flowers/102/>

and we assume a non-commercial research and/or educational use. ImageNet annotations have a non-commercial research and educational license<sup>10</sup>.

PASCAL VOC 2012 images abide by the Flickr Terms of Use<sup>11</sup>.

Cars images have a non-commercial research and educational license<sup>12</sup>

ClipArt, Painting and Sketches are part of the DomainNet dataset which is released under a fair use license<sup>13</sup>.

The ImageNet-A<sup>14</sup> and ImageNet-C<sup>15</sup> images are released with unknown licence, so we refer to the original authors to use these datasets.

---

<sup>10</sup><https://image-net.org/download>

<sup>11</sup><http://host.robots.ox.ac.uk/pascal/VOC/voc2012/>

<sup>12</sup>[http://ai.stanford.edu/~jkrause/cars/car\\_dataset.html](http://ai.stanford.edu/~jkrause/cars/car_dataset.html)

<sup>13</sup><http://ai.bu.edu/DomainNet/#dataset>

<sup>14</sup><https://github.com/hendrycks/natural-adv-examples>

<sup>15</sup><https://github.com/hendrycks/robustness>